RESEARCH ARTICLE

Laser-Induced Forward Transfer Printing on Microneedles for Transdermal Delivery of Gemcitabine

Zoi Kanaki[1†], Chrysoula Chandrinou[2†], Ioanna-Maria Orfanou[1†], Christina Kryou[2], Jill Ziesmer[3], Georgios A. Sotiriou[3], Apostolos Klinakis[1], Constantin Tamvakopoulos[1*], Ioanna Zergioti[2*]

[1]Biomedical Research Foundation Academy of Athens, 4 Soranou Ephessiou Street, 11527, Athens, Greece
[2]Department of Physics, School of Mathematical and Physical Sciences, National Technical University of Athens, Heroon Polytehneiou 9, 15780, Athens, Greece
[3]Department of Microbiology, Tumor and Cell Biology, Karolinska Institutet, SE-171 77, Stockholm, Sweden
[†]*These authors contributed equally to this work.*

Abstract: Cancer treatment with chemotherapeutic drugs remains to be challenging to the physician due to limitations associated with lack of efficacy or high toxicities. Typically, chemotherapeutic drugs are administered intravenously, leading to high drug concentrations that drive efficacy but also lead to known side effects. Delivery of drugs through transdermal microneedles (MNs) has become an important alternative treatment approach. Such delivery options are well suited for chemotherapeutic drugs in which sustained levels would be desirable. In the context of developing a novel approach, laser-induced forward transfer (LIFT) was applied for bioprinting of gemcitabine (Gem) to coat polymethylmethacrylate MNs. Gem, a chemotherapeutic agent used to treat various types of cancer, is a good candidate for MN-assisted transdermal delivery to improve the pharmacokinetics of Gem while reducing efficiency limitations. LIFT bioprinting of Gem for coating of MNs with different drug amounts and successful transdermal delivery in mice is presented in this study. Our approach produced reproducible, accurate, and uniform coatings of the drug on MN arrays, and on in vivo transdermal application of the coated MNs in mice, dose-proportional concentrations of Gem in the plasma of mice was achieved. The developed approach may be extended to several chemotherapeutics and provide advantages for metronomic drug dosing.

Keywords: Laser-induced forward transfer bioprinting; Microneedles; Metronomic chemotherapy; Pharmacokinetics; Transdermal dosing; Sustained drug release

*Correspondence to: Ioanna Zergioti, National Technical University of Athens, Athens GR15780, zergioti@central.ntua.gr; Constantin Tamvakopoulos, Biomedical Research Foundation Academy of Athens, Athens, GR 11527; ctamvakop@bioacademy.gr

Received: December 28, 2021; **Accepted:** February 8, 2022; **Published Online:** February 8, 2022

Citation: Kanaki Z, Chandrinou C, Orfanou IM, *et al*., 2022, Laser Induced Forward Transfer Printing on Microneedles for Transdermal Delivery of Gemcitabine. *Int J Bioprint,* 8(2):554. http://doi.org/10.18063/ijb.v8i2.554

1. Introduction

In the past decades, drug delivery through microneedles (MNs) has become an important approach for treatment when compared to other transdermal methods such as hypodermic needles, topical creams, and transdermal patches. MNs have several advantages over the aforementioned methods such as deeper skin penetration, reduced pain, and increased penetration of high molecular weight drug molecules through stratum corneum, the skin's outermost layer. There are five main ways for active pharmaceutical ingredient (API) delivery[1,2]: (a) API-entrapped in soluble MNs[3-6] (b) API-coated MNs[7], (c) API applied on a patch after the skin has been pierced by solid MNs[8], (d) hollow MNs that enable a continuous fluid flow of the API, and (e) swelling MNs which swell after application and absorption of interstitial fluid, leading to drug diffusion through the swollen MNs[9]. API-coated MNs can be used for delivery of both hydrophilic and hydrophobic drugs[5,10,11]. Their ideal use is for low-dose administration of potent drugs, which are efficacious at low circulating amounts. For example, vaccines applied with MNs induce similar or better immune responses when

© 2022 Author(s). This is an Open Access article distributed under the terms of the Creative Commons Attribution License, permitting distribution and reproduction in any medium, provided the original work is properly cited.

compared to hypodermic needle injections[12]. Despite its advantages, the coating process remains challenging due to limited quantity of the drug coating, the uniformity of the coating, material waste, and the precision in drug dosing. Several technologies have been used in the past, such as dip coating[7,13], gas jet drying[14,15], and spray coating[16,17] with noted limitations[18,19].

In the last decade, three-dimensional (3D) printing technologies have emerged as promising tools for both optoelectronics, and biomedical applications[20]. Through printing methodologies, a plethora of materials can be used with various geometries to achieve a layer-by-layer building of 3D structures. The 3D printing approaches can be used to coat MNs by transferring small microdroplets of the API solution onto the MNs, thus forming uniform layers.

The most noticeable techniques among 3D printing technologies are droplet-based bioprinting (inkjet printing, thermal, piezoelectric, and electrostatic printing), extrusion bioprinting, and laser-induced forward transfer (LIFT). For the coating of MNs for transdermal applications, inkjet printing has been used before[21-23]; however, it has limitations with high viscosity materials, due to excessive force required to eject highly viscous drops. Moreover, inkjet printing is also associated with nozzle clogging[24,25]. In contrast, LIFT[26] is a digital, high-resolution, non-destructive, contactless (nozzle-free) bio-printing technique, which employs single laser pulses to propel the bioink under transfer toward the receiving substrate with high precision. Therefore, LIFT is a promising method used to improve drug coating on MNs with uniform coating layers.

Anticancer chemotherapy drugs (doxorubicin, paclitaxel, methotrexate, etoposide, cisplatin, and gemcitabine [Gem]) are typically associated with non-specific systemic toxicity that leads to patient discomfort and even treatment secession. Gem has been shown to be efficacious against colon, pancreatic, ovarian, breast, head and neck, and lung cancers, in combination with various anticancer agents[27]. However, its poor pharmacokinetics[28] creates a need for alternative approaches for Gem delivery, including encapsulation in nanocarriers (e.g., liposomes, dendrimers, carbon nanotubes, hydrogel[21]) or transdermal patches[29]. Gem's pharmacokinetic and efficacy limitations can be attributed to rapid deactivation and formation of the inactive metabolite 2′,2′-difluoro-2′-deoxyuridine (dFdU) by cytidine deaminase. As Gem is administered based on the classical maximum tolerated dose approach (MTD), initial high doses lead to efficacy. However, such high doses are associated with significant side effects. Furthermore, plasma concentrations of Gem decline rapidly. Patient recovery after treatment necessitates long intervals between doses (3 – 4 weeks, that often lead to disease progression.

Previous studies by our groups have shown that Gem's limitations can be overcome with different strategies. Initially, different targeting peptides were developed and used to generate novel targeted compounds (peptide-Gem conjugate analogs that specifically bound to receptors known to be overexpressed in cancer cells). Such analogs provided us with improved efficacy, pharmacokinetic advantages, and improved toxicity in comparison to equimolar Gem dosing[30-32].

As an extension of the peptide-drug conjugate work, another concept, the metronomic approach (MTR) based on the daily low-dose administration of Gem, was recently evaluated[33]. An oral pro-drug of Gem (OralGem) was chosen for this work in non-small cell lung cancer animal models. We showed that MTR chemotherapy resulted in low circulating and sustained levels of Gem that could potentially lead to the efficacy with less toxicity in comparison to MTD treatments. However, the continuous low-dose supplementation of Gem that is essential for MTR dosing schemes remains a challenge. For example, OralGem is a prodrug of Gem with its own toxicity and dosing limitations due to its first-pass effect[34].

In the effort to search for treatments that provide the optimum efficacy to safety window for cancer patients, a novel concept is presented in this paper. We employed LIFT bioprinting of Gem for coating polymethylmethacrylate (PMMA) MNs with different drug amounts and evaluated the transdermal delivery in mice. Our approach produced reproducible, accurate, and uniform coatings of the drug on the MN arrays, and also yielded dose-proportional concentrations of Gem in mice, following in vivo transdermal application of the coated MNs.

2. Materials and methods

2.1. Materials

Gem hydrochloride was purchased from Carbosynth Limited (Compton, Berkshire, UK). Ammonium acetate, formic acid, and glycerol (≥99.5%) were purchased from Sigma-Aldrich (Sigma-Aldrich Chemie GmbH, Munich, Germany). Acetonitrile (ACN, liquid chromatography [LC-MS] grade) was purchased from Fisher Scientific (Fisher Scientific, Loughborough, UK). Water (LC-MS grade) was purchased from Carlo Erba (Carlo Erba, Milan, Italy). Ketamin was purchased from Richter pharma ag (Austria). Xylazine was purchased from Neocell Pharmaceuticals.

2.2. Gem dispersion preparation

Gem solutions with concentrations of 10, 37.5, and 75 mg/mL were prepared by dissolving Gem in a H_2O: Glycerol solution (90:10 v: v).

Solubility feasibility experiments were conducted to identify the proper solution mixture for the described

studies, since low, medium, high concentrations of drug had to be achieved in a non-toxic solvent system that was compatible with the LIFT technology.

Since Gem is highly soluble in H_2O (>50 mg/mL), we initially tested a range of Gem concentrations (60-80 mg/mL) at 100% H_2O to find the highest soluble concentration. Subsequently, we tested a series of Gem concentrations (60-80 mg/mL) in a mixture of H_2O with a small amount of glycerol (10%). Glycerol contributes to the proper LIFT printing process. Finally, we found that 75 mg/mL was the highest soluble concentration of Gem in a H_2O: Glycerol solution (90:10 v: v).

2.3. MN array fabrication

MN arrays were produced as previously reported[6] using (PMMA, MW 120k, Sigma-Aldrich) which was dissolved at 30 w/v% in ethyl lactate (≥98%, Sigma-Aldrich) for 1.5 h at 150°C. The MN molds (Micropoint Technologies) contained 100 pyramidical cavities with base length and height of 200 μm and 600 μm, respectively. 50 mg of 30 w/v% PMMA was casted on the MN mold, centrifuged for 30 min at 3500 rpm, and left to dry overnight in the fume hood. PMMA MNs were imaged with scanning electron microscopy using a Phenom Pharos microscope (Thermo Fisher Scientific) with 5 kV beam voltage after being sputter-coated with a 5 nm thick carbon nanolayer with the Quorum Q150T (QuorumTech) (**Figure 1**).

2.4. Donor/receiver substrate materials

Quartz substrates coated with 60 nm of Ti were the donor layers and the receiver material was PMMA MNs.

2.5. LIFT process

Printing of Gem solutions was carried out by a solid-state lamp-pumped Nd: YAG (Litron Nano-L 200-10, Neodymium-doped Yttrium Aluminum Garnet, λ = 355 nm, 10 ns pulse duration, UK) and a high-power imaging micromachining system. The imaging system monitored the whole process in real-time through a customized microscope system equipped with a camera, enabling the accurate alignment of the target and substrate materials. A target holder was fixed onto a computer-controlled x–y translation stage with 1 μm positioning resolution and a LabVIEW program was used to synchronize the x–y motion with the laser. The laser beam was controlled by an attenuator while the size of the beam could be adjusted through a variable circular mask. Consequently, a ×15 plano-convex lens was used to focus the laser beam on a donor substrate. The donor substrate was a 1-inch quartz plate coated with a Ti film laser absorbing interlayer, onto which 10 μl of the three Gem solutions (100 μg, 375 μg, and 750 μg) were drop cast. By focusing the laser beam onto the donor substrate, a high-pressure vapor pocket is created in the interface between the Ti layer and the deposited API solution, due to the absorption of the laser pulse from the Ti layer of the donor. This high-pressure vapor pocket expands and propels the supernatant fluid creating a dynamic jet which drives the API solution to the receiver substrate with a high impact velocity, resulting in an nL droplet of Gem solution printed onto the MN substrates for each laser beam pulse. The distance between the donor and the receiver substrates is 700 μm. The laser transfer resulted in a continuous Gem film (5 × 5 mm) on the MNs substrate. The high-speed imaging setup, consisting of a high-speed camera (Photron Europe Limited, FASTCAM Mini-Series AX100 model, High Wycombe, UK) coupled to the system (**Figure 2**); with a maximum recording speed at 540kfps, and a standard LED (Thorlabs LEDD1B) placed opposite of the camera, for illumination purposes. **Figure 2** shows a schematic of the LIFT process for the coating of the PMMA MNs with Gem solution.

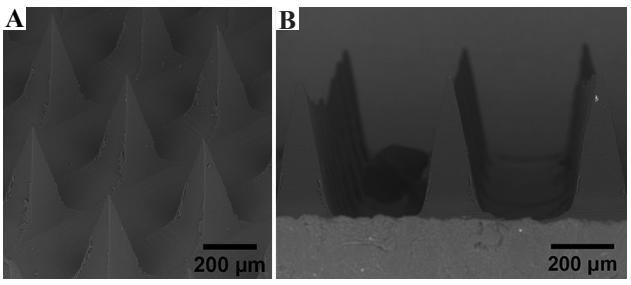

Figure 1. SEM images of PMMA MN arrays tilted at (A) 45° and (B) 90°.

2.6. Statistical analysis

Statistical analysis of the data value distribution was performed by calculating the mean and its standard deviation (SD) from at least 9 individual droplets per LIFT experiment. The results are expressed as mean ± SD. Statistical analyses were performed by the GraphPad Prism 7.0 (GraphPad Software, San Diego, CA, 41 USA).

2.7. Imaging and analysis

The PFV and ImageJ software were utilized to process the captured images.

2.8. Characterization and quantitative analysis of Gem by LC-MS mass spectrometry (MS)

The amount of Gem on the printed areas on the MNs was determined with a high-performance liquid chromatography-tandem mass spectrometry (HPLC-MS/MS). For the identification and quantification of Gem standards and samples, an LC-MS/MS method in MRM mode was developed and validated as described previously[30,31]. HPLC was performed using a Sciex Exion LC system (AB SCIEX LLC, CA, USA) equipped with two pumps, a temperature-

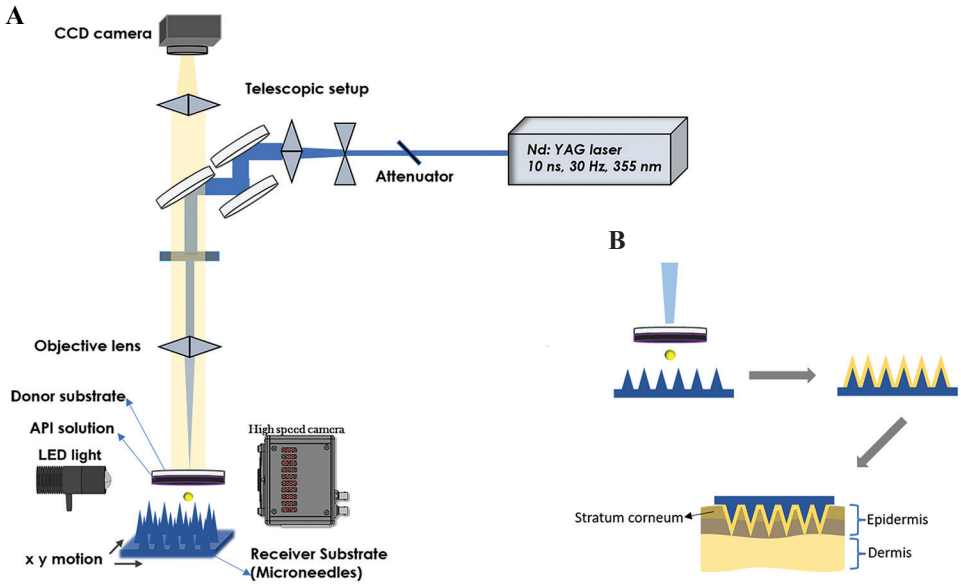

Figure 2. Schematic representation of the LIFT printing process for coating the PMMA MNs. (A) LIFT setup. (B) Coating process.

controlled column compartment, and an autosampler. A dC18 column (Water, Atlantis, 2.1 × 50 mm, 3 µM) was used at a flow rate of 300 µl/min for the separation of analytes of interest. The injection volume of the samples was 10 µl. The mobile phase consisted of A: 100% water, 2 mM ammonium acetate, and 0.1% FA and B: 90% ACN, 10% water, 2 mM ammonium acetate, and 0.1% FA. MS was performed on an API 5500 QTRAP LC-MS/MS system fitted with a Turbo Ion Spray source and a hybrid triple quadrupole/linear ion trap mass spectrometer (AB SCIEX LLC, CA, USA). The standard solutions within a concentration range of 10 – 200 ng/mL of Gem were prepared. Samples of 100, 375, and 750 µg of the initial amount of Gem printed by the LIFT technique were used for the quantification studies. The Gem standards and the laser printed samples on the MN substrates were extracted with MeOH (100%) and then centrifuged with a Speed Vac for 5 min at 16000 rpm. The obtained Gem standards and samples were resuspended in mobile phase A, followed by a 10-fold dilution, and analyzed by HPLC-MS/MS. Warfarin was used as internal standard (IS). The gradient methodology was as follows: 0 – 1.5 min: 100% A, 1.5 – 5 min: 40% A – 60% B, 5 – 10 min: 100% A. The primary MRM transitions for Gem and warfarin were: m/z 264.1→112.0 and 309.1→162.9, respectively. Gem was eluted with a retention time of 1.6 min and the IS was eluted at 5.2 min. Linearity was shown for Gem concentration range of 1–500 ng/mL with a lower on-column detection limit of 10 pg.

2.9. In vivo administration of Gem and extraction of mouse plasma Gem

Mice (C57Bl/6) were purchased from Jackson laboratories and were housed in individually ventilated cages, under specific pathogen-free conditions, in full compliance with Federation of Laboratory Animal Science Associations recommendations in the Animal House Facility of the Biomedical Research Foundation of the Academy of Athens (BRFAA, Greece). All procedures for the care and treatment of the animals were approved by the Institutional Committee on Ethics of Animal Experiments and the Attica Prefecture. No:971840/16-11-21.

Gem was administered to mice either transdermally or intraperitoneally (IP). A total of 36, 5-week-old male mice (average weight 20 g) were used in this study. Prior to the procedure, animals were anesthetized with a Ketamine: Xylazine mix (90 mg/kg Ketamine and 10 mg/kg Xylazine) as previously described[35]. For MN application onto the skin of mice, the left side just above the flank of the mouse was shaved and the MN patch was placed and pressed with the thumb for approximately 2 min and left on the skin for another 10 min without pressure. Manual insertion of MN patches by human volunteers has been reported to be approximately 20 N[4]. PMMA was chosen as the MN polymer based on previous work[6] using PMMA MN tips coated with water-dissolvable, drug-loaded layer which showed that PMMA MNs can be removed successfully from the skin after application. This may reduce toxicity concerns because nonbiodegradable polymers are removed from the tissue after the treatment.

Regarding the transdermal application of Gem, six groups of mice were generated (n≥3) and treated with MNs loaded with 100 µg, 375 µg, or 750 µg of Gem.

Four groups of mice, each composed of 4 individuals were generated to compare intraperitoneal with transdermal application. In the first two groups,

mice were treated with MNs loaded with 10 mg/mL of Gem while mice in another two groups were injected with 10 mg/mL of Gem IP; both dosing routes resulted in 100 μg dose.

Blood was collected from the mouse cheek 15 and 60 min after MN application or IP injection. Blood was placed in heparinized Eppendorf tubes, containing 10 μL heparin (5000 iu/mL), which were then placed immediately on ice and centrifuged for 10min at 3000 rpm. Plasma was then stored in a −80°C freezer prior to analysis. Mice were then euthanized.

Plasma samples (50 μL) were prepared for quantification by protein precipitation with the addition of cold ACN, centrifugation, and evaporation to dryness based on previously reported approach[31]. Gem was determined and quantified by LC-MS/MS analysis as described (see section 2.7). This methodology provided a linear calibration curve with a range of 100–5000 ng/mL for the quantification of Gem in the obtained plasma samples.

3. Results

3.1. LIFT printing of Gem solutions

The direct transfer of the API solution via LIFT printing, which relies on the high velocity and pressure that the liquid droplets have an impact with the MNs substrate, was achieved, resulting in a physical adsorption of the materials onto the substrate. Two-dimensional patterns of continuous Gem layers were printed on the MNs by adjusting the droplet-to-droplet distance to create an even film (**Figure 3**). The photo was taken before the coated material dried. After drying, the difference is not apparent to the naked eye. The purpose is to show that the liquid printed material is evenly distributed and confined within the MN area.

To test process parameters, time-resolved imaging of the printing process was performed by a high-speed camera while the distance between donor and receiver was 700 μm. Different fluences (in the range of 2 J/cm^2 and 250 mJ/cm^2) were investigated to evaluate the process and select the optimum printing conditions. LIFT did not occur at fluences below 380 mJ/cm^2 and above 1530 mJ/cm^2, where the laser energy either produced a small jet and did not transfer the material (subthreshold regime), or it produced a large jet causing a violent ejection of material leading to a disorderly transfer (splashing regime). In the duration of laser transfer, the material that forms the jet is not subjected to any mechanical stress and even though it suffers thermal stress, it only happens during the first few nanometres of bubble formation[36] which does not influence the quality of the transferred material. High-quality laser transfer of a single droplet can only happen in a narrow range of laser fluences which correspond to the optimal regime[37]. In these experiments, the optimum laser fluence was found between 390 and 450 mJ/cm^2, as presented in **Figure 4**.

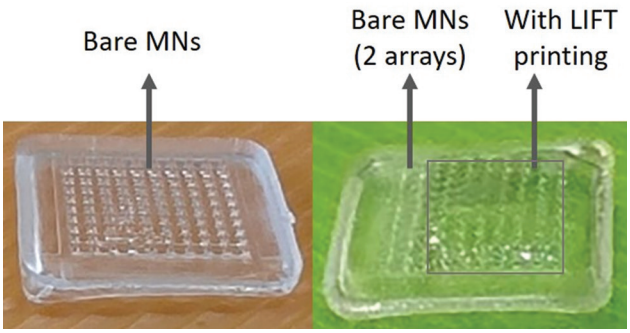

Figure 3. Photograph of the bare MNs substrate (left) and partially just printed Gem-loaded MNs substrate (right).

The impact velocity (0.8 m/s) was calculated by a linear fit of the propagation length of the jet front before impact as a function of the elapsed time of the successive frames captured from the videos. **Figure 5** presents snapshots taken during the printing process by a high-speed camera at four different fluences where successful transfer of the Gem solution occurred.

The droplet size increases with increasing fluence, while higher fluences lead to higher droplet size variation. This may lead to non-uniform deposition film causing the API not to be distributed evenly on the MN patches. It should also be noted that the LIFT technique has the ability to precisely print very small droplets[38] (< 100 pL) of liquids on each MN by adjusting the spot size and fluence for specialized applications. However, the aim of this work was to coat the MNs reproducibly and with a precise amount of Gem.

3.2. Quantification of Gem on the MNs following LIFT printing

LIFT-printed MNs from the three different drug-loaded solutions were analyzed with HPLC-MS/MS to quantify the amount of printed Gem. The results shown in **Figure 6A and B** indicate the average amount of LIFT-Gem: (i) 88 ± 11 μg, (ii) 388 ± 102 μg, and (iii) 1019 ± 100 μg. These values are in good agreement with the theoretical amounts of 100, 375, and 750 μg, suggesting that LIFT enables the precise deposition of API in a reliable and reproducible manner.

It should be noted that a higher than nominal value was observed at the 750 μg dose in comparison to the lower measurements (100 and 375 μg). A limitation of the present study is that at higher doses, solubility leads to a slight increase of the MN loading. Future studies should include more extended trials and optimization at higher doses.

It should be noted that with most conventional drug coating approaches on MNs, the amount of API used

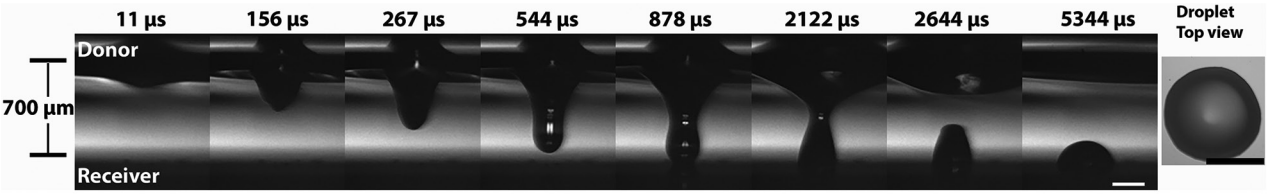

Figure 4. Still frame images extracted from high-speed video of the LIFT printing process for the Gem solution (10 mg/ml). The laser fluence is 390 mJ/cm^2 and the donor-receiver gap is fixed at 700 µm. On the right, a top view of the printed droplet from an optical microscope is shown. The scale bar is 200 µm.

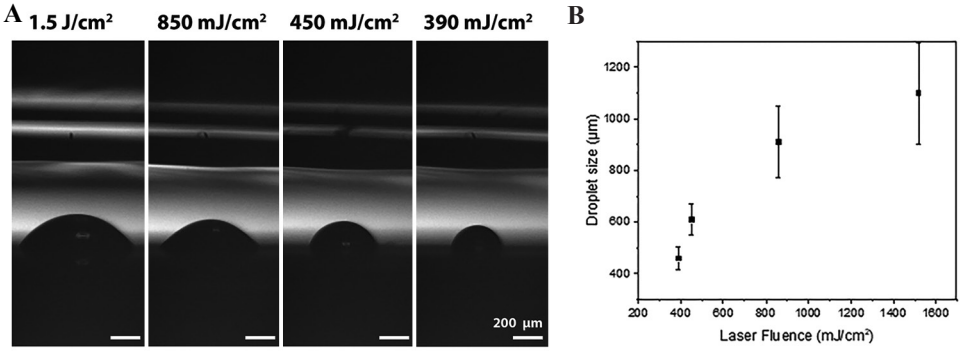

Figure 5. (A) Still frame images of the printed droplet at different fluences extracted from high-speed video. **(B)** Graph showing the relation of the droplet size to the laser fluence.

on the MNs prior to coating is not controlled rather the eventual drug loading is only calculated using loading efficiency equations after the coating is applied[29,34]. The LIFT technique is highly efficient as it only utilizes the amount that is needed for each printing, thus reducing API and solvent waste.

In a study performed by Bhatnagar *et al*.[29], Gem dissolved in phosphate buffer was coated on Zein MNs by a dip-coating technique. In this study, the maximum quantity of drug loaded on the MNs was found at 83 µg, considerably lower than the procedure described herein, where each MN patch could be loaded with up to 750 µg of Gem.

3.3. Gem quantification in mouse plasma

HPLC-MS/MS methodology was utilized to quantify Gem concentrations in the bloodstream of mice treated with MNs loaded with 100, 375, and 750 µg of Gem. A representative HPLC-MS/MS chromatogram for Gem detection in mouse plasma, 15 min after dosing mice with MNs (100 µg dose) is depicted in **Figure 7**.

The use of transdermal MN patches with increasing quantities of Gem leads to higher amounts of Gem in mouse plasma (**Figure 8**). Application of MNs with 100, 375, and 750 µg of Gem in mice led to blood Gem concentrations averaging 479, 1353, and 3067 ng/mL, respectively, at 15 min following dosing. Importantly, Gem levels were increased significantly 1 h after dosing, leading to average blood Gem concentrations of 1087, 1455, and 3803 ng/mL, respectively (**Figure 8B**). The findings from the pharmacokinetic experiments suggested that the administration of Gem through MNs can lead to prolonged systemic exposure. Furthermore, increasing amounts of loaded Gem corresponded well with those found in the bloodstream of treated mice. **Figure 8C** depicts comparative curves of Gem levels, following the increasing dosing in mice.

A comparative study between transdermal delivery and IP injection was performed to further explore the capability of transdermal administration. The IP route was selected for the comparison since it represents a common administration scheme for preclinical efficacy studies in mice. **Figure 9** shows the circulating Gem concentrations after transdermal application and IP delivery of 100 µg Gem in mice. The average amount of LIFT-Gem after 15 min and 60 min were: 479 ± 241 ng/mL and 1087 ± 558 ng/mL respectively, whereas the average amount of IP-Gem after 15 min and 60 min were: 1528 ± 442 ng/mL and 262 ± 12 ng/mL, respectively. These findings are in agreement with previous reports[33] in which 33 µg of Gem was injected IP in mice (Cmax 685 ng/mL, Tmax at 30 min, and rapid decrease within 1 h following the dose). It is important to note that, while IP injection led to decreased Gem levels after 1 h, with the MN transdermal application, a rise in circulating Gem levels was observed.

IP administration of Gem resulted in more than three-fold increase of Gem plasma concentrations 15 min after administration in comparison to the Gem plasma

A

LIFT printed API substance on microneedles	Calculated Gem concentration AVERAGE (μg) ± SD
100 μg (x4)	88 ± 11
375 μg (x4)	388 ± 102
750 μg (x2)	1019 ± 100

B

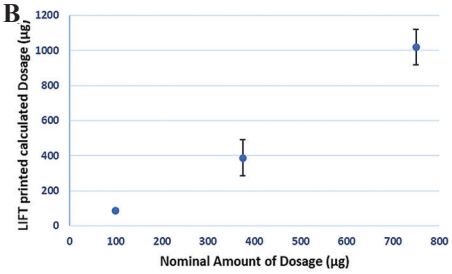

Figure 6. HPLC-MS/MS quantification of Gem on the MNs following LIFT printing. (A) Table presenting the three different Gem concentrations used, the number of repeats of LIFT printing, and the calculated amount of Gem found on the microneedle substrate. (B) Graph showing the LIFT printed calculated dosage related to the nominal amount of Gem.

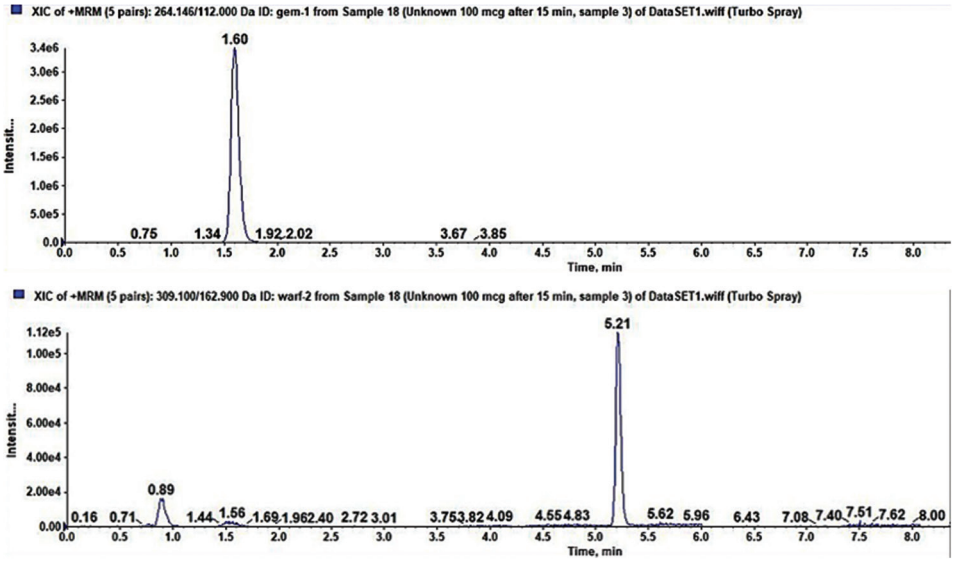

Figure 7. Representative LC-MS/MS chromatograms for Gem detected in mouse plasma, 15min after dosing mice with MNs (100 μg dose). Upper panel: For the detection of Gem, the 264.1/112.0 MRM transition was used (retention time 1.6 min). Lower panel: for the detection of Warfarin used as an internal standard, the 309.1/162.9 MRM transition was used (retention time 5.2 min).

concentrations after MN application. However, within 60 min after IP administration, the Gem concentrations were significantly reduced, while MN transdermal application led to a rise of circulating Gem. This indicates that the MN administration of Gem may have reduced side effects and improved long-term pharmacokinetic profile.

Thus, a sustained release profile might be possible with smaller Gem dosages loaded onto MNs. Indeed, further experimentation is needed to investigate this possibility. Importantly, the average levels of Gem levels in the mouse plasma were found at 1.8 μM and 4.1 μM (479 and 1087 ng/mL) for the 15 and 60 min respectively, even when MNs loaded with a lower dose (100 μg) were used. These concentrations are well above the IC50 of Gem reported for several cancer cell lines (range 20 – 1000 nM[30-33]), suggesting that the efficacy can be achieved in clinically relevant cancer models with the LIFT-coated MNs.

4. Discussion

Current drug manufacturing techniques are performed in specialized factories which follow best practice protocols for mass drug production. Digital printing techniques can be used in medical facilities (i.e., hospitals, medical centers) to maximize the advantage of drug personalization. LIFT method requires a specialized equipment that includes laser, optics, translation stages, and a robot-based pipetting module (under development) for the automated loading of the pharmaceutical compound onto the donor substrate. The cost of LIFT method depends on the automation level and throughput when it comes to the mass production. It offers advantages such as the ability to use any potency and viscosity drug formulations, adaptable resolution (10 – 500 μm) for coating any kind of thin-film substrates including MN patches- as well as individual MNs- and minimal drug formulation waste.

A

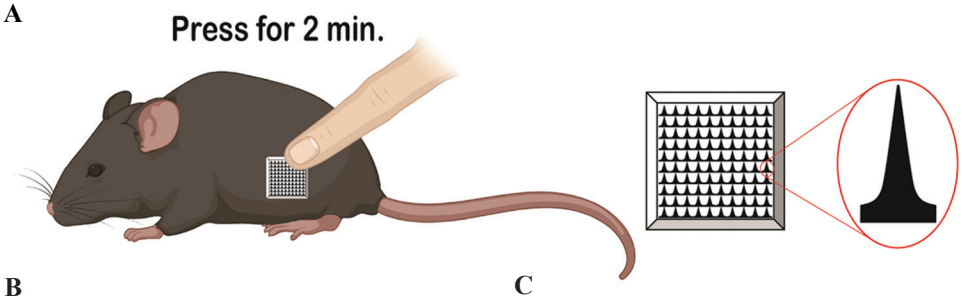

B

Amount of LIFT printed Gem on microneedles	Extraction Time (min)	Gem quantification in mouse plasma AVERAGE (ng/mL) ± SD
100 µg	15	479 ± 241
	60	1087 ± 558
375 µg	15	1353 ± 283
	60	1455 ± 408
750 µg	15	3067 ± 466
	60	3803 ± 206

C

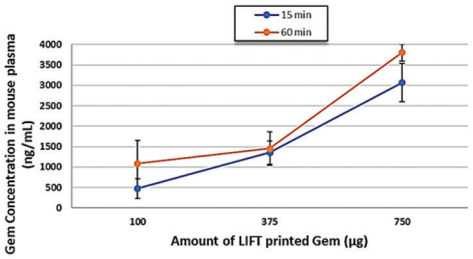

Figure 8. Gem experiments in mice. **(A)** Schematic representation of the in vivo experiment with MNs. MNs application onto the skin of the mouse, on the left side just above the flank. MNs consist of 100 pyramidical cavities with base length 200 µm. The height of each pyramidical cavity is 600 µm. **(B)** Table summarizing the Gem concentrations following dosing, the number of samples, the time point and the Gem concentration in the mouse plasma after transdermal application in mice. **(C)** Graph indicating the correlation between the amount of Gem LIFT loaded in the MNs and the concentration of Gem found in mouse plasma at 15min and 60min.

A

Samples of 100 µg Gem	Calculated Gem concentration in mouse plasma AVERAGE (ng/mL) ± SD
15 min IP (x4)	1528 ± 442
15 min LIFT/microneedles (x4)	479 ± 241
60 min IP (x4)	262 ± 12
60 min LIFT/microneedles (x4)	1087 ± 558

B

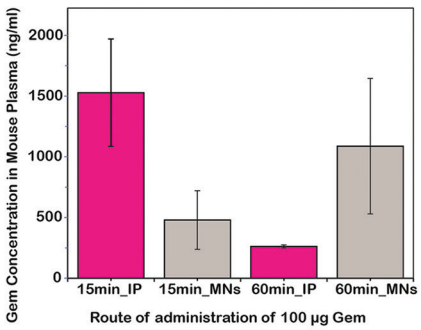

Figure 9. Gem quantification in mouse plasma: MNs versus IP. **(A)** Table presenting the calculated amount of Gem found in mouse plasma after IP injection or transdermal application of 100µg Gem, at 15- and 60-min blood extraction. **(B)** 100 µg of Gem was administered IP and the blood was collected at 15 and 60 min (15_IP, 60_IP). In parallel, the same amount of Gem was administered through MNs and the blood was collected at 15 and 60 min (15_MNs, 60_MNs).

The automated LIFT device is greatly advantageous because it can be used by medical staff offer personalized dosing after minimum training. A laboratory prototype will be built following the optimization process and the validation phase to include the appropriate automation features for the loading of drug formulations and its printing onto the selected substrate (i.e., MN patches).

LIFT printing was employed for the coating of PPMA MNs with (i) 88 µg, (ii) 388 µg, and (iii) 1019 µg of Gem, respectively, for transdermal application in mice. Quantification of the Gem-loaded MNs showed that LIFT printing achieved MN loading with satisfactory reproducibility and accuracy. Unlike most coating techniques, this methodology minimizes drug waste and allows personalized drug dosing with minimum preparation times. It is worth noting, however, that there is a limitation in the amount of drug that can be printed onto the MN patches. Higher Gem doses using the LIFT printing technique as described could not be obtained due to solubility limitations. A maximum 75 mg/mL solution of Gem was achieved in H_2O: Glycerol (90:10 v: v). In future studies, different solutions compatible with the LIFT printing process should be investigated to explore the possibility of higher dosing. Therefore, this method is more suited for potent drugs that are effective at lower dosages. In vivo transdermal application in mice

demonstrated the successful delivery of Gem in the bloodstream for all tested doses. A comparison of MN transdermal application and intraperitoneal injection of 0.1 mg of Gem in mice revealed that the transdermal approach produced similar results but at a slower release rate than the IP. It should be noted that the short half-life of Gem through IP administration as demonstrated by previous reports[33] led to the design of this study protocol by selecting the specific time points. This was also shown in our results (**Figure 9).** However, our results show that the MN approach after 1 h is beneficial, and this will be investigated further.

Although significant Gem concentrations (low μM) were achieved in mouse plasma at the lower Gem dose (100 μg), such concentrations are not expected to lead to toxicity as compared with other administration routes of chemotherapeutics Thus, in comparison with other dosing routes (IP or intravenous dosing), the MNs described here could be an ideal tool for metronomic dosing strategies. The benefits of metronomic dosing can only be achieved with appropriate dosing choices (e.g., oral) since drug administration has to be performed frequently.

The doses tested in this study were those that could be achieved (100 – 750 μg in one MN patch) based on drug solubility in the appropriate vehicle. Dosing in mice ranged from 5 – 37.5 mg/kg (the average weight of mice in the study was 20 g). In order to determine clinical relevance, Gem is dosed in humans as follows: 1000 – 1250 mg/m^2 (approximately 30 – 37.5 mg/kg) as a standard dose of intravenous infusion once a week for 3 – 4 weeks. Alternative dosing schemes for metronomic therapy include a more frequent schedule of every 3rd day with a low-dose infusion of 250 mg/m^2 (7.5 mg/kg) Gem[39]. Clinical studies of the oral availability of Gem have found very low systemic exposure due to rapid first-pass metabolism to dFdU (doses up to 8 mg, or 0.12 mg/kg), suggesting that only a pro-drug approach could be used to provide metronomic Gem with appreciable concentrations following oral dosing[33,40].

5. Conclusions

This work presents a novel approach to coat MN patches in ambient conditions using the LIFT technique. The LIFT process successfully coated PPMA MNs with (i) 88 μg, (ii) 388 μg, and (iii) 1019 μg of Gem for transdermal application in mice, in a reliable and reproducible manner. Application of MNs with the three aforementioned amounts of Gem in mice led to blood Gem concentrations averaging 479, 1353, and 3067 ng/mL respectively, at 15 min and increased considerably after 1h, suggesting that administration of Gem through MNs can lead to prolonged systemic exposure. Furthermore, a comparative study between transdermal delivery and IP injection was performed and the results suggested a sustained release profile with smaller Gem dosages loaded onto MNs and further investigations are underway to explore this possibility. Based on our findings in this study, we believe that MN dosing is a viable alternative to the oral dose. Future studies should include more extended pharmacokinetic protocols as well as their applicability to the preclinical efficacy models to further explore the benefits of the described approach.

Acknowledgments

This research has been co-financed by the European Union and Greek national funds through the Operational Program Competitiveness, Entrepreneurship and Innovation, under the call RESEARCH–CREATE–INNOVATE (project code: T1EDK-00976). G.A.S. acknowledges funding from the European Research Council (ERC) under the European Union's Horizon 2020 research and innovation program (ERC Grant agreement n° 758705). Part of **Figure 8A** has been created using Biorender.com

Conflict of interest

The authors have no conflict of interest to declare.

Author contributions

I.Z., A.K. and C.T. conceived the idea for the project. Z.K. developed the animal models and performed the animal dosing experiments and contributed to the writing of the manuscript. C.C. performed the LIFT high-speed camera experiments for the coating of the MNs, contributed to the LIFT experiments for the coating of the MNs, analyzed the LIFT process data, and also contributed to the writing of the manuscript. I-M.O developed and performed the HPLC-MS/MS quantification methodology and the pharmacokinetics analysis and contributed to the writing of the manuscript. C.K. contributed to the LIFT experiments for the coating of the MNs. J.Z. performed the MN fabrication and contributed in writing - editing. G.A.S. supervised the MN fabrication experiments, analyzed data and contributed to the writing-editing of the manuscript.

References

1. Waghule T, Singhvi G, Dubey SK, *et al*., 2019, Microneedles: A Smart Approach and Increasing Potential for Transdermal Drug Delivery System. *Biomed Pharmacother*, 109:1249–58. https://doi.org/10.1016/j.biopha.2018.10.078
2. Sirbubalo M, Tucak A, Muhamedagic K, *et al*., 2021, 3D Printing a "Touch-Button" Approach to Manufacture Microneedles for Transdermal Drug Delivery. *Pharmaceutics*, 13:924. https://doi.org/10.3390/pharmaceutics13070924

3. Kochhar JS, Quek TC, Soon WJ, *et al*., 2013, Effect of Microneedle Geometry and Supporting Substrate on Microneedle Array Penetration into Skin. *J Pharm Sci*, 102:4100–8. https://doi.org/10.1002/jps.23724
4. Larrañeta E, Moore J, Vicente-Pérez EM, *et al*., 2014, A Proposed Model Membrane and Test Method for Microneedle Insertion Studies. *Int J Pharm*, 472:65–73. https://doi.org/10.1016/j.ijpharm.2014.05.042
5. Larrañeta E, Lutton RE, Woolfson AD, *et al*., 2016, Microneedle Arrays as Transdermal and Intradermal Drug Delivery Systems: Materials Science, Manufacture and Commercial Development. *Mater Sci Eng R Rep*, 104:1–32. https://doi.org/10.1016/j.mser.2016.03.001
6. Ziesmer J, Tajpara P, Hempel NJ, *et al*., 2021, Vancomycin-Loaded Microneedle Arrays against Methicillin-Resistant Staphylococcus Aureus Skin Infections. *Adv Mater Technol*, 6:2001307. https://doi.org/10.1002/admt.202001307
7. Gill HS, Prausnitz MR, 2007, Coated Microneedles for Transdermal Delivery. *J Control Release*, 117:227–37. https://doi.org/10.1016/j.jconrel.2006.10.017
8. Yang Y, Kalluri H, Banga AK, 2011, Effects of Chemical and Physical Enhancement Techniques on Transdermal Delivery of Cyanocobalamin (Vitamin B12) *In Vitro*. *Pharmaceutics*, 3:474–484.
9. Vranic E, Tucak A, Sirbubalo J, *et al*., 2019, Microneedle-based Sensor Systems for Real-time Continuous Transdermal Monitoring of Analytes in Body Fluids. Vol. 73. Cham, Switzerland: Proceedings of the CMBEBIH 2019, IFMBE Proceedings, Springer, p167–172.
10. Pearton M, Saller V, Coulman SA, *et al*., 2012, Microneedle Delivery of Plasmid DNA to Living Human Skin: Formulation Coating, Skin Insertion and Gene Expression. *J Control Release*, 160:561–9. https://doi.org/10.1016/j.jconrel.2012.04.005
11. Zhao X, Coulman SA, Hanna SJ, *et al*., 2017, Formulation of Hydrophobic Peptides for Skin Delivery Via Coated Microneedles. *J Control Release*, 265:2–13. https://doi.org/10.1016/j.jconrel.2017.03.015
12. Tuan-Mahmood TM, McCrudden MT, Torrisi BM, *et al*., 2013, Microneedles for Intradermal and Transdermal Drug Delivery. *Eur J Pharm Sci*, 50:623–37. https://doi.org/10.1016/j.ejps.2013.05.005
13. Ameri M, Kadkhodayan M, Nguyen J, *et al*., 2014, Human Growth Hormone Delivery with a Microneedle Transdermal System: Preclinical Formulation, Stability, Delivery and PK of Therapeutically Relevant Doses. *Pharmaceutics*, 6:220–34. https://doi.org/10.3390/pharmaceutics6020220
14. Chen X, Prow TW, Crichton ML, *et al*., 2009, Dry-coated Microprojection Array Patches for Targeted Delivery of Immune-therapeutics to the Skin. *J Control Release*, 139:212–20. https://doi.org/10.1016/j.jconrel.2009.06.029
15. Chen X, Fernando GJ, Crichton ML, *et al*., 2011, Improving the Reach of Vaccines to Low-resource Regions, with a Needle-free Vaccine Delivery Device and Long-term Thermostabilization. *J Control Release*, 152:349–55. https://doi.org/10.1016/j.jconrel.2011.02.026
16. McGrath MG, Vrdoljak A, O'Mahony C, *et al*., 2011, Determination of Parameters for Successful Spray Coating of Silicon Microneedle Arrays. *Int J Pharm*, 415:140–9. https://doi.org/10.1016/j.ijpharm.2011.05.064
17. Vrdoljak A, McGrath MG, Carey JB, *et al*., 2012, Coated Microneedle Arrays for Transcutaneous Delivery of Live Virus Vaccines. *J Control Release*, 159:34–42. https://doi.org/10.1016/j.jconrel.2011.12.026
18. Bierwagen GP, 1992. Film Coating Technologies and Adhesion. *Electrochim Acta*. 37:1471–8.
19. Gill HS, Prausnitz MR, 2007, Coating Formulations for Microneedles. *Pharm Res*, 24:1369–80. https://doi.org/10.1007/s11095-007-9286-4
20. Alhnan MA, Okwuosa TC, Sadia M, *et al*., 2016, Emergence of 3D Printed Dosage Forms: Opportunities and Challenges. *Pharm Res*, 33:1817. https://doi.org/10.1007/s11095-016-1933-1
21. Uddin MJ, Scoutaris N, Klepetsanis P, *et al*., 2015, Inkjet Printing of Transdermal Microneedles for the Delivery of Anticancer Agents. *Int J Pharm*, 494:593–602. https://doi.org/10.1016/j.ijpharm.2015.01.038
22. Ross S, Scoutaris N, Lamprou D, *et al*., 2015, Inkjet Printing of Insulin Microneedles for Transdermal Delivery. *Drug Deliv Transl Res*, 5:451–61. https://doi.org/10.1007/s13346-015-0251-1
23. Uddin MJ, Scoutaris N, Economidou SN, *et al*., 2020, 3D Printed Microneedles for Anticancer Therapy of Skin Tumours. *Mater Sci Eng C Mater Biol Appl*, 107:110248. https://doi.org/10.1016/j.msec.2019.110248
24. Tarbox TN, Watts AB, Cui Z, *et al*., 2018, An Update on Coating/Manufacturing Techniques of Microneedles. *Drug Deliv Transl Res*, 8:1828–43. https://doi.org/10.1007/s13346-017-0466-4

25. Haj-Ahmad R, Khan H, Arshad MS, *et al*., 2015, Microneedle Coating Techniques for Transdermal Drug Delivery. *Pharmaceutics*, 7:486–502.
https://doi.org/10.3390/pharmaceutics7040486

26. Papazoglou S, Zergioti I, 2017, Laser Induced Forward Transfer (LIFT) of nano-micro patterns for sensor applications. *Microelectron Eng Rev*, 182:25–34.

27. Paroha S, Verma J, Dubey RD, *et al*., 2021, Recent Advances and Prospects in Gemcitabine Drug Delivery Systems. *Int J Pharm*, 592:120043.
https://doi.org/10.1016/j.ijpharm.2020.120043

28. Reid JM, Qu W, Safgren SL, *et al*., 2004. Phase I Trial and Pharmacokinetics of Gemcitabine in Children with Advanced Solid Tumors. *J Clin Oncol*, 22:2445–51.
https://doi.org/10.1200/jco.2004.10.142

29. Bhatnagar S, Kumari P, Pattarabhiran SP, *et al*., 2018, Zein Microneedles for Localized Delivery of Chemotherapeutic Agents to Treat Breast Cancer: Drug Loading, Release Behavior, and Skin Permeation Studies. *AAPS PharmSciTech*, 19:1818–26.
https://doi.org/10.1208/s12249-018-1004-5

30. Karampelas T, Argyros O, Sayyad N, *et al*., 2014. GnRH-Gemcitabine Conjugates for the Treatment of Androgen-independent Prostate Cancer: Pharmacokinetic Enhancements Combined with Targeted Drug Delivery. *Bioconjug Chem*, 25:813–23.
https://doi: 10.1021/bc500081g

31. Karampelas T, Skavatsou E, Argyros O, *et al*., 2017. Gemcitabine Based Peptide Conjugate with Improved Metabolic Properties and Dual Mode of Efficacy. *Mol Pharm*, 14:674–85.
https://doi.org/10.1021/acs.molpharmaceut.6b00961

32. Sayyad N, Vrettos EI, Karampelas T, *et al*., 2019. Development of Bioactive Gemcitabine-D-Lys6-GnRH Prodrugs with Linker-controllable Drug Release Rate and Enhanced Biopharmaceutical Profile. *Eur J Med Chem*, 166:256–66.
https://doi:10.1016/j.ejmech.2019.01.041

33. Skavatsou E, Semitekolou M, Morianos I, *et al*., 2021. Immunotherapy Combined with Metronomic Dosing: An Effective Approach for the Treatment of NSCLC. *Cancers* (*Basel*), 13:1901.
https://doi.org/10.3390/cancers13081901

34. Infante JR, Benhadji KA, Dy GK, *et al*., 2015. Phase 1b Study of the Oral Gemcitabine "Pro-drug" LY2334737 in Combination with Capecitabine in Patients with Advanced Solid Tumors. *Invest New Drugs*, 33:432–9.
https://doi.org/10.1007/s10637-015-0207-9

35. Kanaki Z, Voutsina A, Markou A, *et al*., 2021, Generation of Non-Small Cell Lung Cancer Patient-Derived Xenografts to Study Intratumor Heterogeneity. *Cancers* (*Basel*), 13:2446.
https://doi.org/10.3390/cancers13102446

36. Wang W, Chrisey DB, 2008, Study of Impact-Induced Mechanical Effects in Cell Direct. *J Manuf Sci Eng*, 130:1–10.

37. Theodorakos I, Kalaitzis A, Makrygianni M, *et al*., 2019, Laser-induced forward transfer of high viscous, non-newtonian silver nanoparticle inks: Jet dynamics and temporal evolution of the printed droplet study. *Adv Eng Mater*, 21:1900605.
https://doi.org/10.1002/adem.201900605

38. Makrygianni M, Millionis A, Kryou C, *et al*., 2018, On-Demand Laser Printing of Picoliter-Sized, Highly Viscous, Adhesive Fluids: Beyond Inkjet Limitations. *Adv Mater Interfaces*, 5:1800440.
https://doi.org/10.1002/admi.201800440

39. Pratt SE, Durland-Busbice S, Shepard RL, *et al*., 2013. Efficacy of Low-dose Oral Metronomic Dosing of the Prodrug of Gemcitabine, LY2334737, in Human Tumor Xenografts. *Mol Cancer Ther*, 12:481–90.
https://doi.org/10.1158/1535-7163.MCT-12-0654

40. Veltkamp SA, Jansen RS, Callies S, *et al*, 2008. Oral Administration of Gemcitabine in Patients with Refractory Tumors: A Clinical and Pharmacologic Study. *Clin Cancer Res*, 14:3477–86.
https://doi.org/10.1158/1078-0432.CCR-07-4521

Publisher's note

Whioce Publishing remains neutral with regard to jurisdictional claims in published maps and institutional affiliations.